PROCEEDINGS OF SPIE

SPIEDigitalLibrary.org/conference-proceedings-of-spie

Growth bands in dogfish spines

Stuart Stock, Victoria Cooley, Cindy Tribuzio, Luxi Li, Viktor Nikitin, et al.

Stuart R. Stock, Victoria Cooley, Cindy Tribuzio, Luxi Li, Viktor Nikitin, Olga Antipova, "Growth bands in dogfish spines," Proc. SPIE 12242, Developments in X-Ray Tomography XIV, 122420S (14 October 2022); doi: 10.1117/12.2633826

SPIE.

Event: SPIE Optical Engineering + Applications, 2022, San Diego, California, United States

Growth bands in Pacific dogfish spines

Stuart R. Stock,[a,*] Victoria Cooley[b], Cindy Tribuzio[c],
Luxi Li[d], Olga Antipova[d], Viktor Nikitin[d]
[a] Dept. of Cell and Developmental Biology, Feinberg School of Medicine,
and Simpson Querrey Inst., Northwestern Univ., Chicago, IL, USA;
[b] Dept. of Materials Science and Engineering, Northwestern Univ., Evanston, IL, USA;
[c] Alaska Fisheries Science Center, NOAA Fisheries, Juneau, AK, USA;
[d] Advanced Photon Source, Argonne National Laboratory, Lemont, IL, USA;

ABSTRACT

Dogfish (*Squalus* spp.) possess one or two dorsal-fin spines located at the dorsal midline over the vertebral column. These spines are heavily mineralized, and surface bands of light and dark contrast are used in age determinations. The interior of the spine also contains growth bands visible via optical microscopy of thin sections, but the three-dimensional pattern of growth bands does not appear to have been quantitatively mapped nor has the microstructural origin of the band contrast been established. This paper reports synchrotron microComputed Tomography (microCT) results on spines of *Squalus suckleyi*. MicroCT was performed at beamline 2-BM of the Advanced Photon Source (APS). There are numerous parallel bands, and their contrast consists of varying (higher and lower) values of linear attenuation coefficient, similar to growth bands observed in other mineralized tissues including mammalian cementum and dentin. The microCT data are supplemented by x-ray excited x-ray fluorescence maps of a sectioned Pacific dogfish spine recorded at beamlines 8-BM and 2-ID-E, APS; of particular note are bands of high Zn content, something which has been found in growth bands in other mineralized tissues.

Keywords: dogfish, spines, growth bands, microCT, x-ray fluorescence mapping

1. INTRODUCTION

Elasmobranch skeletons consist of cartilage, and some skeletal tissues of sharks of orders Carcharhiniformes, Lamniformes and Squaliformes are mineralized including vertebral centra and dorsal fin spines (when present). Like tree rings, these centra and spines are recording structures;[1] namely, material is added through the organisms' lifetime, and the tissues preserve the life history of each individual. In mammals, a prominent example of a recording structure is the annual bands in cementum,[2,3] and such growth bands in shark centra are widely used to determine age at death.[4] For dogfish dorsal spines (Fig. 1), age determinations are made using either the ridges on the spine's outer surface or growth bands visible via optical microscopy of polished thin-sections.[5-8]

The optically visible changes in contrast across growth bands result from changes in microstructure, nanostructure and/or elemental or biochemical composition. If the origins of the periodic contrast changes can be deciphered, then it may be possible to infer alterations in underlying biomineralization processes and gain insight into physiological processes and their seasonal variation. Possible variables include mineral density, elemental composition, biochemical composition, microstructure and mineral phase lattice parameters and crystallographic texture. Functional requirements for dogfish spines are quite different than those of shark tessellated tissue[9] or of shark centra. For example, shark centra must accommodate millions of cycles of high amplitude strain.[10,11] Microstructure of the dogfish spine is, therefore, expected to be very different from that of tessellated shark tissues[8] or shark centra.[12,13] Dogfish spines are used for defense and aid locomotion, and functional requirements may be similar to those of shark teeth;[14] however, teeth are frequently replaced whereas spines must survive decades.

* s-stock@northwestern.edu

Developments in X-Ray Tomography XIV, edited by Bert Müller, Ge Wang, Proc. of SPIE Vol. 12242, 122420S
 · 0277-786X · doi: 10.1117/12.2633826

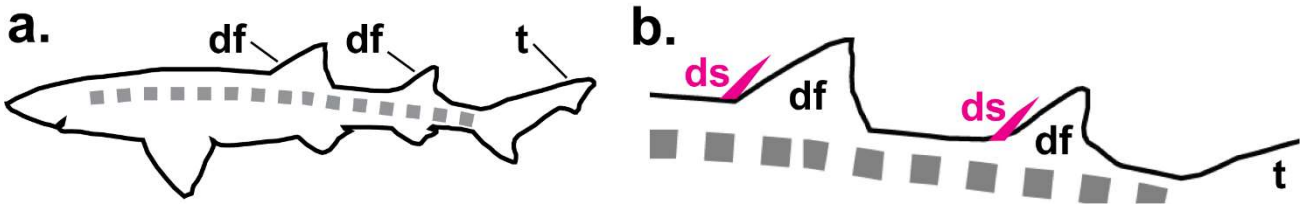

Fig. 1. (a) Schematic of a generalized shark from the side. Dorsal fins "df" and tail "t" are labeled. (b) Enlargement of the central portion of the shark showing the dorsal spines "ds" in magenta.

Absorption contrast in microComputed Tomography (microCT) provides information different from that of optical microscopy of polished thin sections: microCT quantifies the amount of mineral in each reconstructed volume element (voxel) and provides a 3D map of the structure. X-ray excited x-ray fluorescence mapping provides 2D maps of elemental composition on sectioned specimens, something which is quite different from microCT and from optical microscopy. The present study is, to the best of the authors' knowledge, the first microCT and the first x-ray excited x-ray fluorescence mapping study of dogfish spines. The results show prominent growth bands in both modalities, and their description and interpretation form the bulk of this paper.

2. MATERIALS AND METHODS

Several spines and associated soft tissue of the Pacific dogfish *Squalus suckleyi* were kept frozen until they were prepared for characterization. One spine was dissected from soft tissue and was placed immediately in a plastic tube filled with 70% ethanol. The ethanol preserved the spine and prevented it from becoming brittle. Small pieces of plastic packing peanuts were used to hold the spine securely in place for synchrotron microCT imaging. A second spine was also dissected free of soft tissue and was sectioned into ~ 1 mm thick transverse blocks for x-ray excited x-ray fluorescence mapping.

Synchrotron microCT was performed at beamline 2-BM, the Advanced Photon Source (APS).[15] One dogfish spine in its plastic tube was positioned with the spine's axis roughly parallel to the instrument's (vertical) rotation axis. The spine was imaged with 24.35 keV x-ray photons and 3000 projections over 180°. Reconstructions with 0.69 µm volume elements (voxels) required use of a 5x objective lens, the instrument's horizontal field of view with this lens was 1.69 mm, and the spine diameter was larger than this. Two radiographs spanning the diameter of the spine were collected at each viewing angle and stitched together to make a single wider projection. The 4896 x 4896 voxel slices were reconstructed using the 2-BM standard reconstruction software (Tomocupy[16]) with isotropic 0.69 µm voxels. Nine fields of view (FOV) were recorded along the spine's length with 1.30 mm translation between FOV. ImageJ[17]and the BoneJ plugin[18] were used for analysis.

X-ray excited x-ray fluorescence mapping provided maps of elemental composition of transverse sections of the second dogfish spine. This mapping was performed at two APS beam lines with the sections attached to Kapton tape. At beamline 8-BM-B, Kirkpatrick-Baez optics focused the beam of 15.3 keV x-rays to ~ 20 µm diameter.[19] The beam was incident at 45º, and the detector viewed the specimen at the complementary 45º angle. The sample was rastered across the beam, and maps of the fluorescent intensity were recorded. At beamline 2-ID-E, APS, Fresnel optics produced a 0.4-0.45 µm diameter beam of 13.7 keV photons. A small portion of the same section was scanned at much higher resolution than at 8-BM. The 2-ID-E apparatus is described elsewhere.[20]

3. RESULTS AND DISCUSSION

Figure 2 shows synchrotron microCT slices of one dogfish spine with the anterior surface of the spine facing right. The slices span positions 545-550 µm proximal to the spine's tip to 5.75 mm from the tip. Figure 2a shows where the lumen exits the spine, and Fig. 2b shows an enlargement of the area in Fig. 2a around the lumen. Strong phase contrast (narrow white bands) is seen at the air-spine interfaces, and growth bands, alternating bands of light and dark contrast, are prominent and covered two paragraphs below. Contrast within the lumen is complex (see also Fig. 2c) and shows phase contrast of remnants of the spine's unmineralized cartilage core. Although not prominent at the magnification of Fig. 2a,

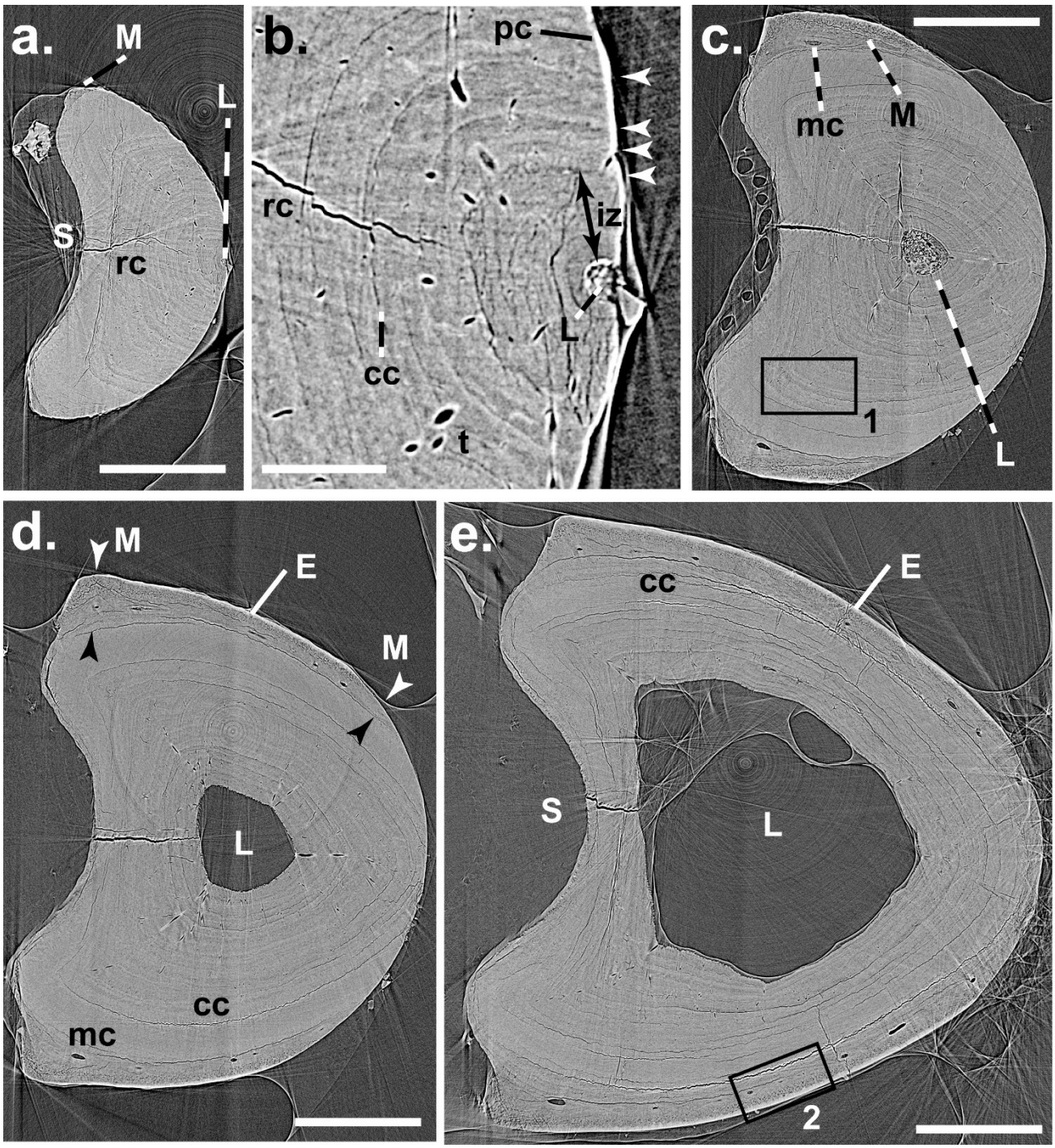

Fig. 2. MicroCT slices showing growth bands. In these and all other slice images, the contrast scale is linear, and lighter the pixel, the more attenuating the corresponding voxel. (a) Slice 545-550 μm from the (distal) tip of the spine. L - lumen; S - sulcus; M – mantle; rc – radial crack. (b) Enlargement of the area surrounding the lumen L in panel a. White horizontal arrowheads – high attenuation growth bands; iz – inner zone surrounding the lumen; cc – circumferential cracks; mc – mantle canal; t – tubules; pc – phase contrast fringes at the air-tissue interface. (c) Slice 1.300 mm proximal from that in panel a. Box 1 is enlarged in Fig. 3. Boundaries of the mantle - black/white pairs of arrows; E – enameloid. (d) Slice 1.300 mm proximal from that in panel c. (e) Slice 2.600 mm proximal from that in panel d. Box 2 is enlarged in Fig. 3. The scale bars in panels (a, c-e) are 500 μm in length and that in panel b is 100 μm long.

an inner zone "iz" of mineralized tissue surrounding the lumen is present (Fig. 2b) and is less attenuating than the surrounding tissue. A wide radial crack is present in all of the slices as are a number of circumferential cracks. Tubules radiating from the lumen are seen surrounding it in Fig. 2a-c. The lumen has a roughly circular cross-section in Fig. 2a and its diameter is 30-35 μm. In the 1.3 mm to the position of Fig. 2c, the lumen cross-section has become larger and has taken an egg-like shape with major and minor diameters of about 255 μm and 155 μm, respectively. In the next 1.3 mm (Fig. 2d), the lumen has become more polygonal; the maximum and minimum diameters (defined by the largest circle touching the outermost edges of the lumen and by the smallest circle fitting completely within the lumen, respectively) are 465 μm and 368 μm, respectively. The lumen covers about 1% of the cross-sectional area in Fig. 2c, about 5% in Fig. 2d and about 25% in Fig. 2e. In the ~6 mm proximal of Fig. 2e (data not shown), the outer dimensions of the spine increase slowly relative to the increase in size of the lumen.

In Fig. 2a, the mantle region is barely present within the lateral tips of the spine cross-section. At a position 1.3 mm proximal from that of Fig. 2a, mantle covers just over 50% of the lateral and anterior surfaces (Fig. 2c). At a position 2.6 mm proximal from that of Fig. 2a, mantle covers about 75% of the lateral and anterior surfaces (Fig. 2d). At a position 5.2 mm proximal from that of Fig. 2a, mantle covers all the lateral and anterior surfaces (Fig. 2e).

In all of the slice images, growth bands are seen as concentric light and dark circumferential contrast; four of these are identified by horizontal white arrowheads in Fig. 2b. The widths of the higher attenuation bands (white) are highly variable, and the thinnest of these are 4-7 voxels wide (3-5 μm). Figure 3a shows enlarged area 1 of Fig. 2c, and the linear attenuation coefficient was measured at 16 points within the light band labeled by the red bar and the same number measured in the dark band labeled with the yellow bars. The mean linear attenuation coefficient ± one standard deviation was 2.4 ± 0.5 cm^{-1} for the light band and 1.7 ± 0.5 cm^{-1} for the dark band. Note that contrast within the bands was quite noisy. When the measurements are repeated on the median value for 11 adjacent slices, the mean does not change but the standard deviation drops to 0.3 cm^{-1}. Based on the 11-slice average and the difference of over two standard deviations between medians for light and dark bands, the authors conclude that mineral levels are significantly different in the two bands. The mineralized portion of the wedge volume of a typical shark centrum (scalloped hammerhead, imaged at 2-BM at the same energy, same number of points placed only on the mineralized tissue) has a mean linear attenuation coefficient of 3.9 ± 1.0 cm^{-1}.[21] For comparison, bone's mass attenuation coefficient at this x-ray energy is about 2.2 cm^2/g (interpolation between listed NIST table values for a bone standard[20]) and for bone densities 1.9 or 2.0 g/cm^3, the linear attenuation coefficient is 4.2 or 4.4 cm^{-1}, respectively. Therefore, dogfish spines have a lower mineral density than the mineralized volume of shark centra or bone. A possible functional advantage of the uniform structure (at the level of 0.69 μm voxels) and the lower mineral density compared to bone and shark centra tissue is discussed below.

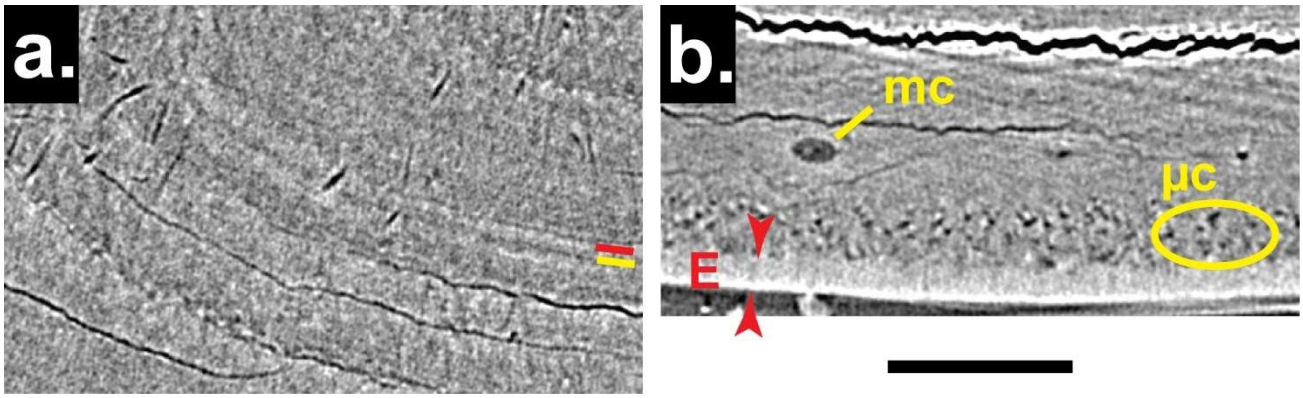

Fig. 3. (a) Enlargement of box 1 of Fig. 2c. Linear attenuation coefficient values were measured along the light band (marked by the red bar) and the adjacent dark band (marked by the yellow bar). (b) Enlargement of box 2 in Fig. 2e; note the rotation of the panel relative to the full slice. The red arrowheads indicate the thickness of the enameloid layer "E". The yellow ellipse surrounds several microcanals labeled "μc". mc – mantle canals; The two panels are at the same scale, and the scale bar shows 100 μm.

Figure 3b, the enlargement of box 2 in Fig. 2e, contains two prominent circumferential cracks; the wider crack at the top of the image has a white phase contrast fringe comparable to that at the spine surface (near the bottom of the image). A layer of lighter contrast (higher mineral density) is seen at the spine surface; it extends beyond the phase contrast fringe and has a width of 20-25 μm and mean linear attenuation coefficient (several hundred voxels) of 3.6 ± 0.8 cm^{-1} compared with 2.0 ± 0.6 cm^{-1} for the nearby mantle tissue. The outer layer is consistent with enameloid described by others.[5-8] A mantle canal "mc" and a layer of microcanals "μc", some of which are surrounded by the yellow ellipse, are also present in this region. Microcanal cross-sections are quite variable, but their dimensions are typically 5-10 μm. Figure 4 shows segmentation of the microcanals over a small subvolume extending through 124 slices; the 3D rendering (Fig. 4c) shows them extending through this volume and parallel to the spine axis.

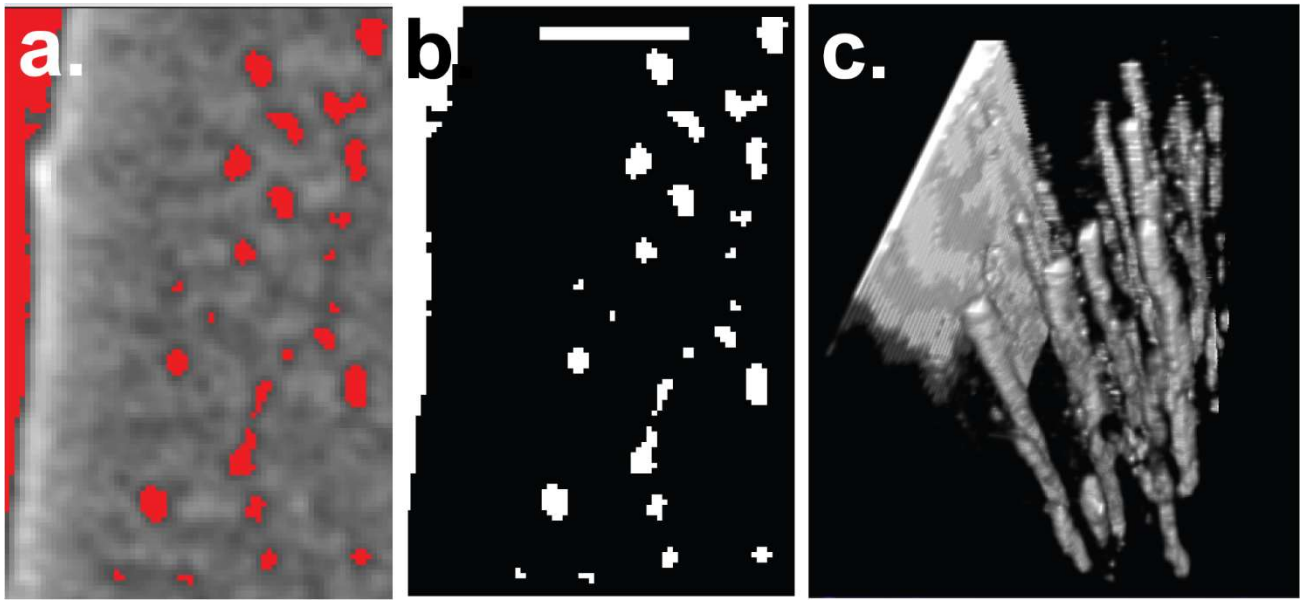

Fig. 4. Typical microcanal region of the dogfish spine. (a) Grayscale image with segmented volume superimposed in red. (b) Segmented slice with void space shown white and solid as black. (c) 3D rendering of the void space extending 124 voxels along the spine axis. The scale bar equals 20 μm.

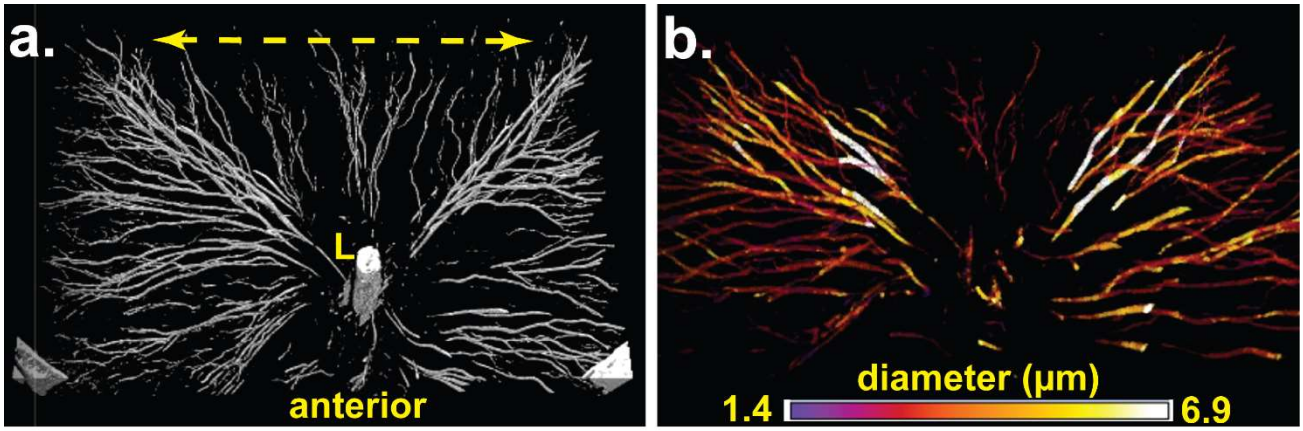

Fig. 5. 3D renderings of tubules within a 201-slice thick volume. Both renderings are at approximately the same viewing angle and magnification. (a) Low attenuation voxels shown as solid. (b) Vessel diameter color coded using BoneJ and the color table shown at bottom of the right-hand panel.

Figure 5 shows 3D rendering of the tubules extending from the lumen. The volume is approximately midway between the slices in Fig. 2a and 2c and extends over 201 slices. Figure 5a shows a simple rendering of all of the vessel voxels; many of the vessels seem to end in space, but this is because they extend out of the subvolume. Note that the vessels are much sparser in the posterior section of this subvolume (dashed yellow line). Figure 5b shows the vessels labeled with their diameters as determined by BoneJ. The diameters range from 2 voxels (1.4 μm) to 10 voxels (6.9 μm), and the mean diameter is 3.1 ± 0.9 μm. These tubules occupy about 0.7% of the subvolume.

Figure 6 shows Ca, Zn, P and composite (Ca+Zn+P) scanning fluorescence maps (red, green, blue and all three, respectively) of a section cut from a dogfish spine recorded at 8-BM, APS. For each elemental map, the maximum and minimum number of counts per sec (cts/s) appear in the upper right and lower right of that panel. There is a slight cutting-related valley in the surface and an accompanying surface-related dip in all three intensities (solid white bar in the Zn map of Fig. 6). The lumen (L) is at the right side of the map. Five or six concentric bands of increased Zn intensity are present, but the width, spacing and intensity of these bands vary.

Figure 7 also shows Ca, Zn, P and composite (Ca+Zn+P) scanning fluorescence maps (red, green, blue and all three, respectively) of a small area of a dogfish spine recorded at 2-ID-E, APS. For each elemental map, the maximum; minimum number of counts per sec (cts/s) appear in the lower right of that panel. Twelve bands of increased Zn intensity are present (marked by white disks) and are concentric, following the spine's outer surface. Most of these bands are paired, i.e., two bands surround a narrow lower intensity (dark) band with wider bands of lower intensity to either side of the pair. In the lower right portion of this map, the higher intensity band arrangement appears more complex than simple pairs of bands, and there may be an additional band not marked.

One large radial crack runs from the middle of the exterior surface of the sulcus; this crack extends though the volume covered in Fig. 2 but has ended before the proximal end of the volume imaged (data not shown). One expects that if this crack were formed during dissection, prying of the spine from the surrounding tissue would have affected the proximal sulcus more than the distal portion. One suspects that this radial crack was formed pre-dissection and probably in vivo.

The presence of many circumferential cracks throughout the volume of the spine indicates that it is strongly resistant to fracture. In vivo, the spine probably experiences impact loading, both compression and bending. Under loading, a relatively stiff structure of mineralized tissue would eventually nucleate one or more cracks at its outer surface, cracks which would then propagate into the structure at an acute angle to the surface under tension and lead to loss of part of the spine. If the spine were loaded from its anterior side (convex in *S. suckleyi*), cracks would link to this surface (left in Fig. 2); if loading were from the posterior (i.e., the concave surface), then cracks would emanate from this surface. Although further observations are required, the observed concentric cracks are parallel to the growth bands and remain far from and largely unlinked to the spine's outer surface. This suggests that there is a layered microstructure which delaminates under large in vivo loads and which limits the likelihood of fracture. As spines are not repaired or replaced, this hypothetical mechanism may have evolved to help spines survive for decades.

As noted above, mineral density in the spine is lower than that of the cone's mineralized subvolume in the shark centrum and that of cortical bone tissue. Lower mineral levels suggests that the volume fraction of cartilage is higher

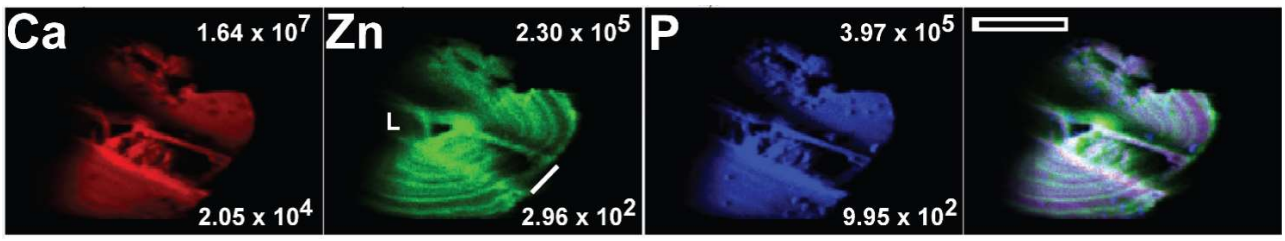

Fig. 6. X-ray excited scanning fluorescence map of Ca, Zn and P intensities (red, green, blue, respectively) along with a composite Ca+Zn+P of the three intensities. The intensity scale is linear, and the brighter the color, the greater the intensity. The map of this section of dogfish spine was recorded at 8-BM, APS. The maximum and minimum x-ray intensities (cts/s) are given at the upper right and lower right of each panel, respectively. The scale bar is 1.00 mm long.

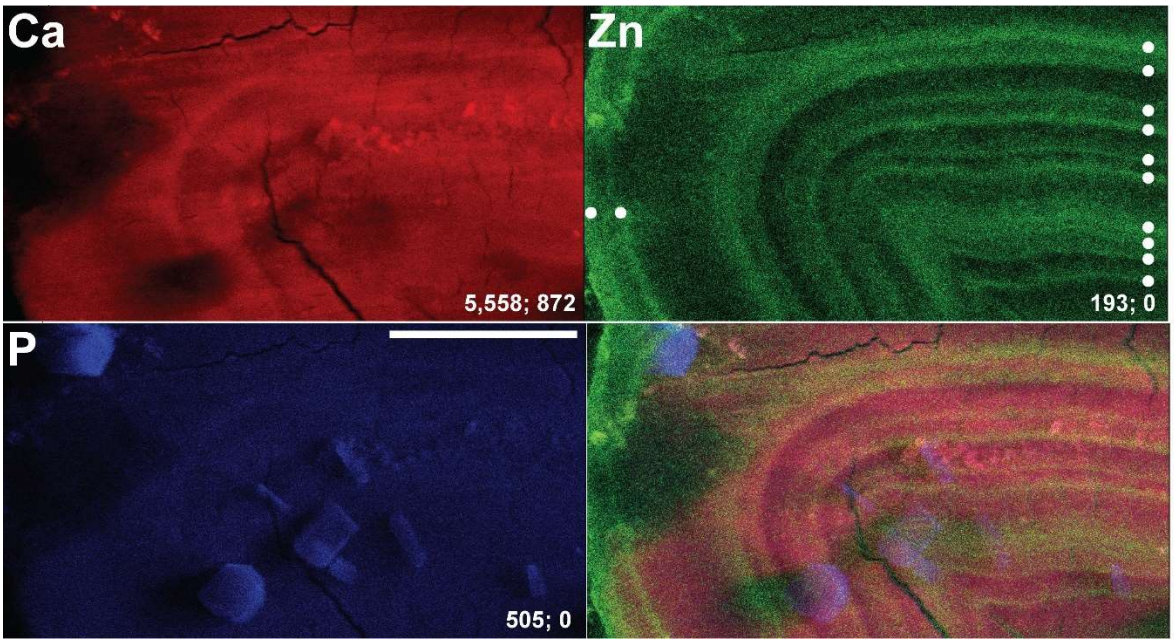

Fig. 7. X-ray excited scanning fluorescence map of Ca, Zn and P intensities (red, green, blue, respectively) along with a composite Ca+Zn+P of the three intensities. The intensity scale is linear, and the brighter the color, the greater the intensity. The map of this area of a dogfish spine was recorded at 2-ID-E, APS. The maximum; minimum x-ray intensities (cts/s) are given at the lower right of each panel. The white disks mark bands of increased Zn intensity. The scale bar is 200 µm long.

in the dogfish spine than in the mineralized portions of shark centra. Typically, higher mineral content corresponds to stiffer tissue, but, in the case of dogfish spine vs centrum comparison, this inference may be inaccurate because the centrum contains a significant interconnected volume of unmineralized tissue. Examination of published synchrotron microCT data of the wedge of a blue shark's centrum[13] reveals "only" 41 vol% mineralized tissue. This very open structure may have evolved to be more compliant than a volume content with the same mineralized tissue but little to no included porosity, i.e., the dogfish spine.

This initial characterization of growth band structure (synchrotron microCT and x-ray fluorescence maps) reveals complexity requiring further analysis. Spines from additional animals should be studied as well as spines from other species. Synchrotron microCT was very recently performed on the blocks mapped with x-ray fluorescence, but painstaking co-alignment must be completed before data of the two modalities can be directly compared. If dogfish spines contain mineralized cartilage (as expected), then small angle scattering of spine tissue and observation of D-period peaks (produced by bioapatite mineral phase "decorating" cartilage fibers and the resulting ordering of bioapatite nanoparticles like in centra tissue[23]) would confirm this. Observation of cracks within more spines would help clarify their role in fracture resistance. Whether the cracks occur at specific microstructural features or at positions dictated solely by solid mechanics remains an open question. Higher resolution synchrotron microCT or scanning electron microscopy might reveal an answer.

ACKNOWLEDGEMENTS

This research used resources of the Advanced Photon Source, a U.S. Department of Energy (DOE) Office of Science User Facility, operated for the DOE Office of Science by Argonne National Laboratory under Contract No. DE-AC02-06CH11357. Argonne National Laboratory's work was supported by the U.S. Department of Energy, Office of Science, Office of Basic Energy Sciences, under contract DE-AC02-06CH11357. Samples were provided by staff on the Alaska Fisheries Science Center annual groundfish longline survey.

REFERENCES

[1] Klevezal, G.A. [Recording Structures of Mammals]. Rotterdam: Balkema (1996).
[2] Stock, S.R., Finney, L.A., Telser, A., Maxey, E., Vogt, S., and Okasinski, J.S. "Cementum structure in Beluga whale teeth," Acta Biomater 48, 289-299 (2017).
[3] Naji, S., Rendu, W., and Gourichon, L. Eds. Cementum in Anthropology, Cambridge Univ. Press: Cambridge (2022).
[4] Natanson, L.J., Skomal, G.B., Hoffmann, S.L., Porter, M.E., Goldman, K.J., and Serra, D. "Age and growth of sharks: do vertebral band pairs record age?" Mar Freshwater Res 69, 1440-1452 (2018).
[5] Beamish, R.J., and McFarlane, G.A. "Annulus development on the second dorsal spine of the spiny dogfish (*Squalus acanthias*) and its validity for age determination," Can J Fish Aquat Sci 42, 1799-1805 (1985).
[6] Irvine, S.B., Stevens, J.D., and Laurenson, L.J.B. "Comparing external and internal dorsal-spine bands to interpret age and growth of the giant lantern shark, *Etmopterus baxteri* (Squaliformes: Etmopteridae)," Environ Biol Fish 77, 253-264 (2006).
[7] Clarke, M.W., and Irvine, S.B. "Terminology for ageing of chondrichthyan fish using dorsal-fin spines," Environ Biol Fish 77, 273-277 (2006).
[8] Maisey, J.G. "Finspine morphogenesis in squalid and heterodontid sharks," Zool J Linnean Soc 66, 161,183 (1979).
[9] Seidel, R., Roschger, A., Li, L., Bizzarro, J.J., Zhang, Q., Yin, J., Yang, T., Weaver, J.C., Fratzl, P. Roschger, P., Dean, M.N. "Mechanical properties of stingray tesserae: High-resolution correlative analysis of mineral density and indentation moduli in tessellated cartilage," Acta Biomater 96, 421-435 (2019).
[10] Porter, M.E., Diaz, C., Sturm, J.J., Grotmol, S., Summers, A.P., and Long, J.H., Jr. "Built for speed: strain in the cartilaginous vertebral columns of sharks," Zool 117, 19-27 (2014).
[11] Ingle, D.I., Natanson, L.J., and Porter, M.E. "Mechanical behavior of shark vertebral centra at biologically relevant strains," J Exp Biol 221, 188318 (2018).
[12] Morse, P.E., Stock, M.K., James, K.C., Natanson, L.J., and Stock, S.R. "Shark vertebral microanatomy and mineral density variation studied with laboratory microComputed Tomography," J Struct Biol 214, 107831 (2022).
[13] Stock, S.R., Morse, P.E., Stock, M.K., James, K.C., Natanson, L.J., Chen, H., Shevchenko, P.D., Maxey, E.R., Antipova, O.A., and Park, J.-S. "Microstructure and energy dispersive diffraction reconstruction of 3D patterns of crystallographic texture in a shark centrum," J Medical Imaging 9, 031504 (2022).
[14] Amini, S., Razi, H., Seidel, R., Werner, D., White, W.T., Weaver, J.C., Dean, M.N., and Fratzl, P. "Shape-preserving erosion controlled by the graded microarchitecture of shark tooth enameloid," Nature Comm 11, 5971 (2020).
[15] Nikitin, V., Tekawade, A., Duchkov, A., Shevchenko, P., and De Carlo, F. "Real-time streaming tomographic reconstruction with on-demand data capturing and 3D zooming to regions of interest," J Synchrotron Radiat 29, 816-828 (2022).
[16] Nikitin, V. "Tomocupy," https://tomocupy.readthedocs.io/en/latest/ accessed 07/15/2022.
[17] Rasband, W. and other contributors. "ImageJ," Version 1.53q, Fiji implentation. https://imagej.nih.gov/ij/ accessed 07/19/2022.
[18] Domander, R., Felder, A.A., and Doube, M. "BoneJ2 - refactoring established research software," Wellcome Open Research, 6, 37 (2021).
[19] Kujala, N., Marathe, S., Shu, D., Shi, B., Qian, J., Maxey, E., Finney, L., Macrander, A., and Assoufid, L. "Kirkpatrick-Baez mirrors to focus hard X-rays in two dimensions as fabricated, tested and installed at the Advanced Photon Source," J Synchrotron Rad 21, 662 - 668 (2014).
[20] Brister, E.Y., Vasi, Z., Antipova, O., Robinson, A., Tan, X., Agarwal, A., Stock, S.R., Carriero, A., and Richter, C.-P. "X-ray fluorescence microscopy: A method of measuring ion concentrations in the ear," Hearing Res 391, 107948 (2020).
[21] Hubbell JH, Seltzer SM. "Tables of X-Ray Mass Attenuation Coefficients and Mass Energy-Absorption Coefficients from 1 keV to 20 MeV for Elements $Z = 1$ to 92 and 48 Additional Substances of Dosimetric Interest," NISTIR 5632. (2004) https://dx.doi.org/10.18434/T4D01F accessed 7/17/2022.
[22] Stock, S.R., James, K.C., Natanson, L.J. and Shevchenko, P. Unpublished data, 2-BM, APS (2020).
[23] Park, J.-S., Almer, J.D., James, K.C., Natanson, L.J., and Stock, S.R., "Mineral in shark vertebrae studied by wide angle and by small angle x-ray scattering," J Roy Soc Interface revision under review (July 2022).